J. Fluid Mech. (1991), *vol.* 227, *pp.* 617–640
Printed in Great Britain

Relaxation behind shock waves in ionizing neon

By T. J. McINTYRE†, A. F. P. HOUWING, R. J. SANDEMAN AND H.-A. BACHOR

Department of Physics and Theoretical Physics, Faculty of Science, Australian National University, Canberra, Australia

(Received 1 February 1990 and in revised form 20 October 1990)

Experiments in ionizing neon are described in which heavy-particle and electron densities are measured and compared with the current kinetic model. The experimental results allow a determination of the atom–atom collisional excitation cross-section constant, giving a value of $(8\pm2)\times10^{-20}$ cm^2/eV for the range of conditions examined. The population of two of the excited-state levels of the atom are measured and compared with theoretical predictions. The experimental populations are found to follow the expected behaviour in the quasi-equilibrium region, but are several orders of magnitude higher than predicted in the non-equilibrium zone. These findings suggest that the depopulation of excited states through ionizing collisions occurs more slowly than expected. Absorption linewidths and line shifts are also measured in the quasi-equilibrium region and found to compare well with theory. A small precursor population is also observed and population measurements in this region are compared with other experimental results in argon and krypton.

1. Introduction

There has been considerable investigation of excitation and ionization behind shock waves in monatomic gases, particularly argon. (See, for example Petschek & Byron 1957; Harwell & Jahn 1964; Kelly 1966; Wong & Bershader 1966; Oettinger & Bershader 1967; McLaren & Hobson 1968; Demmig 1977; Liu, Whitten & Glass 1978; Glass & Liu 1978; Liu & Glass 1979; Liu, Takayama & Glass 1980; Bötticher, Müller & Schneider 1981; Bötticher & Kilpin 1984). A successful model to describe the relaxation and recombination processes has been developed, yielding an experimental determination of the atom–atom collisional excitation cross-section constant, S^*_{A-A}. Glass & Liu (1978) found for argon, $S^*_{Ar-Ar} = 1.0\times10^{-19}$ cm^2/eV while Glass, Liu & Tang (1977), using an identical method, obtained for krypton, $S^*_{Kr-Kr} = 1.2\times10^{-19}$ cm^2/eV. In both experiments disturbances were observed which perturbed the flow behind the shock wave and in extreme cases the shock itself. The disturbances hindered the measurements of the cross-section constants as the conditions were no longer truly one-dimensional. In an effort to remove the flow instabilities observed in their experiments, Glass & Lui (1978) added small amounts of hydrogen to the test gas which, while helping to stabilize conditions, also had the effect of reducing the relaxation length, owing to the collisional properties of the hydrogen. For argon, the instability was completely removed for impurity levels of 0.5% H_2 (by volume) and larger, while for krypton, stability was obtained at about 0.4% H_2, but further increase resulted in a return to unstable conditions. These

† Current address: DLR, ES, Bunsenstr. 10, 3400 Göttingen, Germany.

observations plus others from related experimental work has led to significant research efforts in the area of shock wave instability. (See, for example, Alieva & Andreev 1987; Bedin 1989; Fowles & Houwing 1984; Grigor'ev *et al.* 1986; Henderson 1987, 1988; Houwing, Fowles & Sandeman 1983; Houwing *et al.* 1986; Kuznetsov, 1986, 1990; Kuznetsov & Sarrov 1989; Liu 1986; McIntyre *et al.* 1987, 1989; Mishin *et al.* 1981; Munz 1987; Ni, Sugak & Fortov 1987; Yushchenkova 1980; and Yushchenkova, Mishin & Roshchin 1985.)

Many instability theories exist but few are applicable to the shock-induced ionization discussed here. A theory which does have relevance to shock wave instability associated with ionization relaxation is the *Anomalous Relaxation Theory* proposed by Baryshnikov & Skvortsov (1979). They suggested that a sufficiently strong exothermic stage in the overall endothermic process creates disturbances in the flow, while Mishin *et al.* (1981) suggested, for ionizing gases, that energy stored in metastable states of the atom and in excited states of molecular ions is later released, destabilizing the flow. However, Houwing *et al.* (1986) monitored the populations of these states for both stable and unstable conditions and found that insufficient energy was available to cause the instability. An upper limit was set on the population in the relaxation zone which was well below that predicted for instability by Yushchenkova (1980) and Yushchenkova *et al.* (1985). They also measured populations in the equilibrium zone which agreed well with the accepted model for ionization. No other instability theory has produced a successful explanation, and thus the problem remains unsolved.

Although considerable investigation has been carried out in argon and to a lesser extent in krypton, little work has been done in neon. Its relatively high ionization limit means that much stronger shocks are required to produce a significant electron population. Early studies of shock-induced ionization have relied strongly on interferometric measurements (see, for example Glass & Lui 1978) to provide information on relaxation processes in the non-equilibrium zone. More recently, Houwing *et al.* (1986) have used the hook method to measure excited-state-populations in ionized argon. Although providing important information on these populations in the quasi-equilibrium region, their method was not sufficiently sensitive to measure populations in the non-equilibrium region. McIntyre *et al.* (1987, 1989) were able to achieve much larger sensitivities using an infrared diode laser to measure the populations of metastable and non-metastable levels of argon in the non-equilibrium zone through absorption and make some important observations in relation to shock wave stability, excited-state populations and relaxation processes. In particular, they noted that the excited-state populations directly behind the shock did not agree with predictions based on the currently accepted theory. Specifically they did not satisfy the modified Saha equation used in earlier work by Oettinger & Bershader (1967). However, since both non-metastable and metastable populations behaved in a similar way for both stable and unstable shock waves, no correlation with the Anomalous Relaxation Theory was found. It was deduced, therefore, that the ionization of excited atoms occurred more slowly than implied by the theoretical work of Oettinger & Bershader.

The absorption technique utilized by McIntyre *et al.* (1987, 1989) has only been possible since the emergence of narrowband tunable lasers. Ring dye lasers allow probing of transitions in the visible spectrum while diode lasers allow access to the infrared. Narrowband absorption has advantages over broadband absorption in that it provides not only accurate measurements of the populations of internal energy levels but also yields information on the broadening and shifting of the absorption

line. These parameters are related to the translational temperature and the pressure, allowing their measurement provided the absorption line has been investigated under known conditions. Hansen, Salimian & Rea (1983) provide an overview of the technique with several different lasers examining such species as NO and CO in shock tube flows. Monatomic gases also have transitions accessible by such systems. McIntyre *et al.* (1989), as well as determining populations, were able to measure linewidths of some of the transitions lines in argon using an infrared diode laser and make comparisons with theoretical predictions of Stark and Doppler broadening. However, because of the tuning characteristics of the diode laser, the measurements were restricted to a narrow region centred on the absorption line. The large numbers of electrons liberated at the electron cascade front made it difficult to accurately measure the lineshape at the end of the relaxation zone because of the considerable increase in Stark broadening. McIntyre *et al.* (1987) inferred linewidths in this region by making measurements away from line centre with a different diode and also with broadband measurements, but a high accuracy can only be obtained by a full range of detuning about the line centre.

In contrast to argon, which has most of its absorption lines in the ultraviolet and the infrared, neon offers some reasonably strong lines in the visible region of the spectrum. These lines are easily accessed using a tunable ring dye laser, which does not suffer from the same mode hopping problems as the diode lasers and should thus give better resolution of the line profiles. Measurements of the metastable and non-metastable populations in regions where there are large electron densities should thus be more accurate than in the argon case, enabling determination of the level populations and the Stark broadening. For measurements between the shock and cascade front, absorption can be measured on the line centre and theoretical widths utilized to infer populations. One of the aims of this work is thus to examine the relaxation and quasi-equilibrium regions behind a normal shock wave in neon using a tunable ring dye laser capable of much wider tunability than in the argon experiments. Another aim is to measure electron and heavy particle densities using dual-wavelength interferometry for comparison with the current kinetic model to obtain a value for the atom–atom excitation cross-section $S^*_{\mathrm{Ne-Ne}}$.

2. Theoretical considerations

2.1. *Ionizing gas flow*

The development of a kinetic model has led to a two-temperature description of the relaxing gas. The translational shock front immediately excites the heavy particles to a high Maxwellian temperature, T_{A}, placing the gas in a state of chemical non-equilibrium. Harwell & Jahn (1964) have shown that ionization is dominated by a two-state process involving an initial rate-controlling excitation followed by rapid ionization. Demmig (1983) and Meyer–Prüssner (1983) have suggested that in the early stages of ionization, the electrons follow a truncated Maxwellian velocity distribution since the high-velocity electrons lose their energy in inelastic collisions with atoms. These collisions produce further electrons through ionization of the atoms. The subsequent electrons are lower in energy, much of it having been spent in overcoming the ionization potential. Initially the population of the depleted high-energy tail is slow because of the low electron–electron collision rate, but at larger electron densities, this collision rate is sufficiently fast to maintain a Maxwellian temperature T_{e}. This temperature is substantially lower than the atom and ion temperature T_{A} because energy transfer between heavy particles and electrons via

elastic collisions is extremely inefficient. Ionization through electron–atom collisions, being dependent on both electron temperature and density, is initially slow, but increases rapidly once sufficient electrons are present to increase the energy transfer rate. Consequently, reactions involving these collisions begin to dominate. The larger collisional cross-section together with the mobility of the electrons rapidly brings the gas to equilibrium in the region known as the electron cascade front (ECF). Beyond this, the gas cools owing to radiative recombination processes and bremsstrahlung at a rate sufficiently slow for the chemical reactions to maintain equilibrium.

The governing equations describing a mixture of heavy particles and electrons are as follows:

$$(N_A+N_e)\,u = N_0\,u_0, \tag{1a}$$

$$m_A(N_A+N_e)\,u^2+N_e\,kT_e+(N_A+N_e)\,kT_A = m_A\,N_0\,u_0^2+N_0\,kT_0, \tag{1b}$$

$$\frac{d}{dx}[\tfrac{1}{2}m_A(N_A+N_e)\,u^3+\tfrac{5}{2}(N_A+N_e)\,kT_A\,u+\tfrac{5}{2}N_e\,kT_e\,u+N_e\,k\theta u] = -Q_R, \tag{1c}$$

$$\tfrac{3}{2}N_e\,uk\frac{dT_e}{dx}+N_e\,kT_e\frac{du}{dx} = \eta+\phi, \tag{1d}$$

$$\frac{d(N_e\,u)}{dx} = \frac{dN_e}{dt}, \tag{1e}$$

where u is the velocity, m is the mass, N the number density, T the temperature, and θ is the atom ionisation temperature. Subscripts A, e and 0 denote atom, electron and initial conditions respectively. To solve these equations it is necessary to provide models for the production rate of electrons, dN_e/dt; the rate at which thermal energy is given to the free electrons through elastic collisions, η; the rate at which thermal energy is given to the free electrons through inelastic collisions, ϕ; and the radiative energy loss Q_R. The description of these processes is much the same for each of the monatomic gases. Glass & Liu (1978) and Glass *et al.* (1977) discuss, in detail, these parameters for argon and krypton. Here only the details particular to neon are presented.

The reactions which produce and remove electrons throughout the flow can be summarized in the single reaction.

$$A+M \underset{k_{rM}}{\overset{k_{fM}}{\rightleftharpoons}} A^+ + e^- + M,$$

where M is an atom or an electron; and k_{fM} and k_{rM} are the forward and reverse reaction rate parameters respectively. The relatively high excitation temperature of the monatomic gases as compared to the plasma temperature means that only reactants with kinetic energy just above threshold contribute to excitation. Experimental measurements have shown that cross-sections of this type vary linearly with energy, just above threshold, and hence the rate of the excitation can be written (see Glass *et al.* 1977) as

$$k_{fM}(T_M) = S^*_{A-M}\left[\frac{32}{\pi}\left(\frac{m_A+m_M}{m_A\,m_M}\right)\right]^{\frac{1}{2}}(kT_M)^{\frac{3}{2}}\left(\frac{\theta^*_A}{2T_M}+1\right)\exp\left(\frac{-\theta^*_A}{T_M}\right), \tag{2}$$

where m is the mass of the particle; T_M the temperature of the collision partner; θ^*_A the excitation temperature of A; and S^*_{A-M} is the excitation cross-section constant for excitation of A by a collision with M.

To describe the reaction processes, numerical values for the atom–atom, S^*_{A-A}, and atom–electron, S^*_{A-e}, cross-sections must be supplied. For argon and krypton, values for S^*_{A-e} from Zapcsochnyi & Felston (1966) have been used. More recently Machodo, Leal & Csanak (1984) using electron impact considerations have calculated values for S^*_{A-e} for most of the lower-lying excited states of neon. Since excitation may be to any of these levels, we obtain the atom–electron cross-section constant by summing over all the levels presented, allowing for small differences in energies. These values are presented in table 1. The atom–atom excitation cross-section constant can then be determined by comparing theoretically predicted relaxation lengths with experimentally measured values as has been done for argon and krypton.

With these parameters the net production rate for electrons can be written

$$\left(\frac{\mathrm{d}N_e}{\mathrm{d}t}\right)_M = k_{fM} N_A N_M - k_{rM} N_M N_e^2 = k_{fM}(T_M) N_M \left[N_A - \frac{N_e^2}{K_{eq}^{MA}(T_M)}\right], \tag{3a}$$

with

$$\frac{\mathrm{d}N_e}{\mathrm{d}t} = \left(\frac{\mathrm{d}N_e}{\mathrm{d}t}\right)_A + \left(\frac{\mathrm{d}N_e}{\mathrm{d}t}\right)_e, \tag{3b}$$

where $K_{eq}^{MA}(T_M)$ is the equilibrium constant for collisions with particle M as given by Hoffert & Lien (1967). Introducing an equilibrium constant at temperature T_M is justified here since recombination reactions only become significant once thermal equilibrium has been established.

The rate for energy transfer to the electrons through elastic collisions, η, is the sum of the rate at which energy is transferred by atoms and the rate at which it is transferred by ions. These are, in turn, dependent on the momentum transfer cross-sections Q_{eA} and Q_{ei} respectively. From neon, we use the same form of Q_{ei} as that used for argon and krypton (equation 15 in Glass & Liu 1978). Itikawa (1974) has measured momentum transfer cross-sections for electron collisions with atoms and molecules over a wide range of energies. His results for argon, krypton, and xenon all feature a characteristic dip called the Ramsauer minimum. Neon does not exhibit this effect in the energy regime we consider and the cross-section is simply a slowly increasing function of energy. Following the analysis of Itikawa and fitting curves to his results gives

$$Q_{eA}(T_e) = \begin{cases} \dfrac{10^{-16}}{kT_e}(1.20\times10^{-4}T_e)\ \mathrm{cm}^2 & \text{for } T_e < 3500\ \mathrm{K}, \quad (4a) \\ \dfrac{10^{-16}}{kT_e}(-0.92+4.08\times10^{-4}T_e)\ \mathrm{cm}^2 & \text{for } T_e \geqslant 3500\ \mathrm{K}, \quad (4b) \end{cases}$$

where kT_e has the units of eV.

Finally, we consider the energy loss in the quasi-equilibrium zone which results from continuum and line radiation. Since there are many energy levels with uncertain oscillator strengths in the atom, it is difficult to determine the magnitude of the line radiation. Horn, Wong & Bershader (1967) have shown that line and continuum contributions for argon are of the same order of magnitude. Glass *et al.* (1977) presumed the total radiation energy loss to be

$$Q_R = (1+a)\,Q_C, \tag{5}$$

where a is a constant, and Q_C is the continuum energy loss as calculated by Oettinger & Bershader (1967). We presume the same form for neon, initially using a value of unity for the parameter a.

Level (Paschen notation)	Excitation energy (eV)	Integral cross-section σ_I (cm^2)	Energy at σ_I (eV)	S^*_{Ne-e} (cm^2/eV)
$1s_2$	16.85	1.44×10^{-18}	20.00	4.6×10^{-19}
$1s_3$	16.71	3.05×10^{-19}	20.00	9.3×10^{-20}
$1s_4$	16.67	9.73×10^{-19}	20.00	2.9×10^{-19}
$1s_5$	16.61	1.53×10^{-18}	20.00	4.5×10^{-19}
$2p_1$	18.96	1.64×10^{-18}	22.13	5.2×10^{-19}
$2p_3$	18.70	3.66×10^{-20}	22.13	1.1×10^{-20}

TABLE 1. Atom–electron excitation cross-section constants for lower-lying levels of neon. S^*_{Ne-e} (total) $= 1.6\times10^{-18}$ cm^2/eV.

The evaluation of the population of excited atomic states has been considered by a number of authors (see Bates, Kingston & McWhirter 1962; Byron, Stabler & Bortz 1962; Oettinger & Bershader 1967). They assume that collisions with electrons are sufficient to maintain the atomic energy states above a certain principal quantum number in a Boltzmann distribution at the temperature of the free electrons. For argon, this cut-off level closely matches the first excited state and hence all excited states are presumed to have this distribution. Since neon has a similar electronic configuration and we are considering similar energies, it is reasonable to assume that all the excited states of neon follow the same distribution. Oettinger & Bershader (1967) derived a 'modified' Saha equation that related the population of an excited state q to the electron number density, viz.

$$N(q) = \frac{N_e^2 h^3}{2(2\pi m_e kT_e)^{1.5}} \frac{g(q)}{Q_i(T_e)} \exp\left[\frac{I-E_q}{kT_e}\right], \tag{6a}$$

where N_e is the electron number density, $g(q)$ is the degeneracy of state q, E_q its excitation energy, I the ionization potential, and Q_i the partition function of the ion. The ion is considered to be only in one of its two ground states and hence, for neon,

$$Q_i(T_e) = 4+2\exp\left[\frac{-1124}{T_e}\right]. \tag{6b}$$

2.2. *Dual-wavelength interferometry*

The refractive index of a plasma depends on contributions from atoms, electrons and ions. While the effect of heavy particles is to increase the refractive index n, the presence of electrons causes a decrease. Since the contributions are different at different wavelengths, one is able to separate the two effects by probing the plasma with two separate-wavelength lasers and thus deduce both the heavy particle and electron populations. The equations relevant to our work give the heavy-particle density ρ and electron number density N_e as

$$\rho = \rho_0 + \frac{S_1\lambda_1 A_2 - S_2\lambda_2 A_1}{(G_1A_2 - G_2A_1)L}, \tag{7a}$$

$$N_e = \frac{S_1\lambda_1 G_2 - S_2\lambda_2 G_1}{(G_1A_2 - G_2A_1)L}, \tag{7b}$$

where S is the dimensionless fringe shift, L the path length, G the Gladstone–Dale coefficient, ρ_0 the density ahead of the shock, and A (in c.g.s. units) is the quantity

$$A_j = 4.49 \times 10^{-14} \lambda_j^2 + (1-r)\, G_j\, m_A. \tag{8}$$

Here r is the ratio of the ion-to-atom Gladstone–Dale coefficients and subscripts $j = 1, 2$ refer to measurements at laser wavelength λ_1 and λ_2 respectively. Leonard (1974) has measured values for the dispersion of light by neon, and for our wavelengths $\lambda_1 = 488.0$ nm and $\lambda_2 = 770.0$ nm he finds $G_1 = 0.0755$ cm^3 g^{-1} and $G_2 = 0.0750$ cm^3 g^{-1}.

Values for r are less well tabulated. Alpher & White (1959) calculate for argon a value of 0.67 while Tang (1977) uses 0.75 for krypton. No value has been provided for neon, and lacking any experimental determination, we presume $r = 0.67$ for neon also. While the error in this assumption may be as large as 50%, the effect on experimental measurements is greatly diminished by the relatively low contribution to the fringe shift by ions.

2.3. *Absorption*

Assuming non-saturated absorption, the initial laser intensity I_0 is reduced to I, after passing through a plasma of thickness L with

$$\frac{I}{I_0} = \exp\{-k_\nu L\}, \tag{9}$$

where k_ν is the absorption coefficient for the gas at frequency ν. In order to determine an excited-state population by measuring the absorption, it is necessary to examine how k_ν, is affected by the absorption line profile. Following Traving (1968) one can write

$$k_\nu = \frac{\pi e^2}{m_e c} f N_{ex} P(\Delta\nu)\left[1 - \exp\left(\frac{-h\nu_0}{kT_e}\right)\right], \tag{10}$$

where N_{ex} is the population of the absorbing energy level, f is the oscillator strength of the transition, $P(\Delta\nu)$ describes the shape and magnitude of the absorption line profile dependent on the detuning $\Delta\nu$ from line centre, ν_0 is the centre frequency of the transition, and the last term in square brackets accounts for stimulated emission.

The profile of the line is determined by a number of different broadening mechanisms. Those that are important in the present work are Doppler broadening, and three types of pressure broadening: resonant, Van der Waals, and Stark. With a knowledge of all these mechanisms it is possible to determine the form for the line profile $P(\Delta\nu)$. For Doppler broadening, the line profile is Gaussian:

$$P_D(\Delta\nu) = \frac{1}{\pi^{\frac{1}{2}} \Delta\nu_D} \exp\left[-\left(\frac{\Delta\nu}{\Delta\nu_D}\right)^2\right], \tag{11}$$

where $\Delta\nu$ is the detuning of the incident light from line centre, and $\Delta\nu_D$ is the width, given by

$$\Delta\nu_D = \frac{1}{\lambda_0}\left(\frac{2kT_A}{m_A}\right)^{\frac{1}{2}}. \tag{12}$$

For pressure broadening, the profile is Lorentzian:

$$P_L(\Delta\nu) = \frac{1}{2\pi} \frac{\gamma}{(\Delta\nu)^2 + \gamma^2/4}, \tag{13}$$

where $\Delta\nu$ is again the detuning allowing for any line shift, and γ is the full width at half maximum (FWHM) of the profile. Resonance broadening occurs from interactions between the absorbing atom and other atoms of the same type. It can only occur when one of the energy levels involved is connected radiatively with the ground state. Traving (1968) determines the FWHM for this type of broadening to be

$$\gamma_{\mathrm{R}} = \frac{e^2 f_{\mathrm{R}} \lambda_{\mathrm{R}} N}{4 m_{\mathrm{e}} c}, \tag{14}$$

where f_{R}, λ_{R} are the oscillator strength and wavelength, respectively, of the resonant transition and N is the ground-state population. Resonance broadening does not affect metastable levels as no resonant transition exists. Van der Waals broadening is similar to resonance broadening except that it results from interactions with all non-resonant atoms. Griem (1964) determines the FWHM for this broadening to be

$$\gamma_{\mathrm{VDW}} = N\left(\frac{9\pi\hbar^5 \overline{R_\alpha^2}}{16 M^3 E_{\mathrm{p}}^2}\right)^{\frac{2}{5}} \overline{v^{\frac{3}{5}}}, \tag{15}$$

where N is the ground-state population; $\overline{R_\alpha^2}$ is the square of the coordinate vector of the radiating electron given by Griem; M the mass of the perturbing atom; E_{p} the energy of the nearest resonant level and $\overline{v^{\frac{3}{5}}}$ is an average velocity calculated by

$$\overline{v^{\frac{3}{5}}} = \frac{2}{\pi^{\frac{1}{2}}}\left(\frac{2kT_{\mathrm{A}}}{M}\right)^{\frac{3}{10}} \times 0.93. \tag{16}$$

Stark broadening results from interactions of the absorbing atom with charged particles. Extensive theoretical work on this type of broadening has been performed by Griem (1964) and reviewed by Wiese (1965) and Griem (1974). Two types of approximation are used to determine the broadening. The impact theory presumes very fast interactions between the atom and charged particle resulting in a line profile that is approximately Lorentzian. Obviously this type of approximation is best suited to the light electrons. The second approach, the quasi-static method presumes the interaction to occur over the whole time that the atom is emitting or absorbing and is applicable to the slower-moving ions. The effect of this interaction is to introduce some asymmetry to the line profile but for our work this is presumed to be small. As well as causing a broadening of the line profile, this type of interaction introduces a significant shift of the absorption line profile away from the normal wavelength of the line. The formulae that are used to calculate the FWHM, γ_{ST}, and shift δ_{ST} (in c.g.s. units) are

$$\gamma_{\mathrm{ST}} = 2[1 + 1.75\times10^{-4} N_{\mathrm{e}}^{\frac{1}{4}} \alpha (1 - 0.068 N_{\mathrm{e}}^{\frac{1}{6}} T_{\mathrm{A}}^{-\frac{1}{2}})] \times 10^{-24} w N_{\mathrm{e}} \frac{c}{\lambda_{\mathrm{L}}^2}, \tag{17a}$$

$$\delta_{\mathrm{ST}} = \left[\frac{d}{w} + 2.0\times10^{-4} N_{\mathrm{e}}^{\frac{1}{4}} \alpha (1 - 0.068 N_{\mathrm{e}}^{\frac{1}{6}} T_{\mathrm{A}}^{-\frac{1}{2}})\right] \times 10^{-24} w N_{\mathrm{e}} \frac{c}{\lambda_{\mathrm{L}}^2}, \tag{17b}$$

where N_{e} is the number density of electrons, λ_{L} the wavelength of the line and w, d/w, and α are the width, shift-to-width ratio, and ion broadening parameters respectively. These are tabulated over a wide number of transition lines by Griem. Their values are taken directly from Griem's tables (with appropriate interpolation for temperature). Allowances for different electron number densities are already incorporated in the above equations.

To combine the profiles from Doppler and pressure broadening we must form a Voigt profile. For such a profile,

$$P(\Delta\nu) = \int_{-\infty}^{\infty} P_{\mathrm{L}}(\Delta\nu - z)\, P_{\mathrm{D}}(z)\, \mathrm{d}z = \frac{1}{\pi^{\frac{1}{2}}\Delta\nu_{\mathrm{D}}} H(\alpha, v). \tag{18}$$

Here $H(\alpha, v)$ is the Voigt function

$$H(\alpha, v) = \frac{\alpha}{\pi} \int_{-\infty}^{+\infty} \frac{\mathrm{e}^{-y^2}}{\alpha^2 + (v-y)^2} \mathrm{d}y, \tag{19}$$

where $v = \Delta\nu/\Delta\nu_{\mathrm{D}}$ is a measure of the detuning from line centre, and

$$\alpha = \frac{\gamma_{\mathrm{R}} + \gamma_{\mathrm{VDW}} + \gamma_{\mathrm{ST}}}{2\Delta\nu_{\mathrm{D}}} \tag{20}$$

is a measure of the Lorentz broadening to Doppler broadening ratio.

In the present experiment, three separate regions are considered. In the precursor region there are very small numbers of electrons and ions and hence Stark broadening can be ignored. The absorption line is a Voigt profile with contributions from Doppler, resonant, and Van der Waals broadening. The second region is the relaxation zone. Throughout this region, the electron population is increasing and Stark broadening becomes comparable to the other broadening mechanisms. The profile is still a Voigt function but has contributions from all the mechanisms mentioned above. The third region is the quasi-equilibrium zone. In this region of the flow, the ionization fraction is of the order of 10 % and Stark broadening dominates. Stark widths are an order of magnitude larger than any other contributions and the line is assumed to have a Lorentzian profile only.

3. Experimental arrangement

3.1. *Shock tube conditions*

All experiments were conducted in the department's double-diaphragm shock tube (DDT) operated in single diaphragm mode (see Sandeman & Allen 1971). Before each shot, the shock tube was evacuated using a silicon oil diffusion pump backed by a rotary roughing pump to below 0.1 Pa, flushed with neon, and then re-evacuated to better than 0.1 Pa. It was then filled with the desired initial pressure of neon and allowed to sit for only about two minutes before the tube was fired. Driver conditions were chosen to obtain Mach numbers in the range $17 < M_{\mathrm{s}} < 21$.

3.2. *Flow visualization*

Flow visualization was used to examine the stability of conditions throughout the various regions of the flow. The experimental arrangement is shown in figure 1. An excimer laser–pumped-dye laser described by Pulford (1987) was used to generate a 50 ns light pulse, sufficiently short to 'freeze' the flow. The beam was focused through an optical fibre to remove the laser's spatial coherence and then imaged through a Carl Zeiss Mach-Zehnder interferometer. One arm of the interferometer contains the test section where the gas emerges from the end of the shock tube. The laser light was then imaged onto photographic film through an aperture and a filter, which were used to discriminate against luminosity from the gas flow.

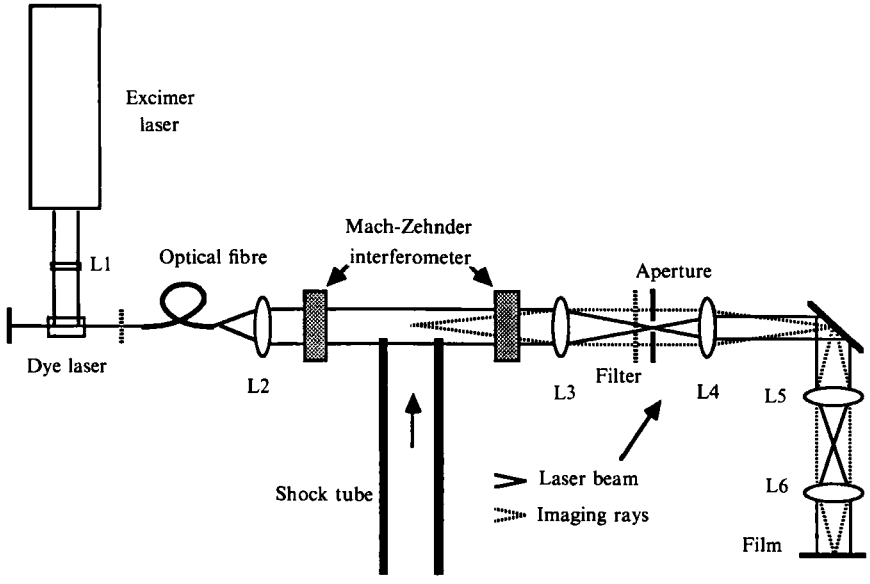

FIGURE 1. Experimental arrangement for flow visualization. Components: L1, Quartz cylindrical lens, $f = 300$ mm; L2, Glass spherical lens, $f = 200$ mm; L3, Glass spherical lens, $f = 1000$ mm; L4, Glass spherical lens, $f = 200$ mm; L5, Glass spherical lens, $f = 50$ mm; L6, Glass spherical lens, $f = 200$ mm. Dye: Rhodamine 6G – 0.001 Molar. Filter: Wavelength – 590 nm $\pm$ 1.8 nm. Film: Ilford HP5 Sheet.

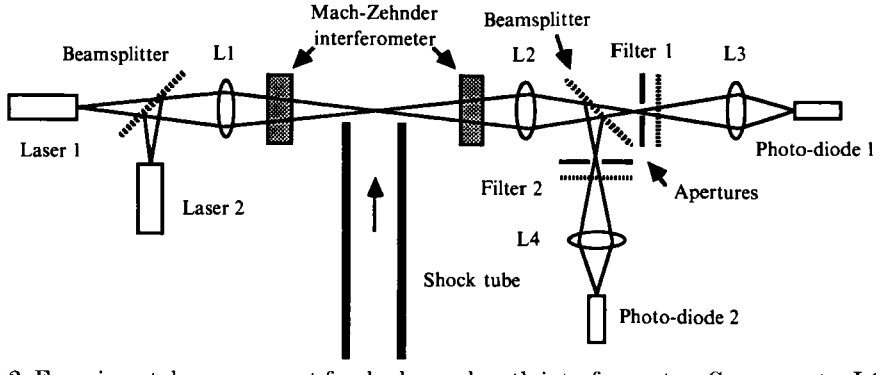

FIGURE 2. Experimental arrangement for dual-wavelength interferometry. Components: L1, Glass spherical lens, $f = 1000$ mm; L2, Glass spherical lens, $f = 1000$ mm; L3, Glass spherical lens, $f = 300$ mm; L4, Glass spherical lens, $f = 300$ mm; Lasers: Ar–ion, diode. Filters: 488 nm, 772 nm. Bandwidths: 1 nm, 5 nm.

3.3. *Dual wavelength interferometry*

The experimental arrangement for dual-wavelength interferometry is shown in figure 2. Two laser beams were combined and focused through the Carl Zeiss Mach-Zehnder interferometer into the gas emerging from the end of the shock tube. The light was then separated back into its two wavelengths and focused onto photodiodes each with a frequency response greater than 20 MHz. Each beam was passed through apertures and filters to discriminate against luminosity from the flow. Fringe counting was time-resolved with an accuracy better than 0.1 of a fringe. To best determine the heavy-particle and electron populations it is desirable to have the laser

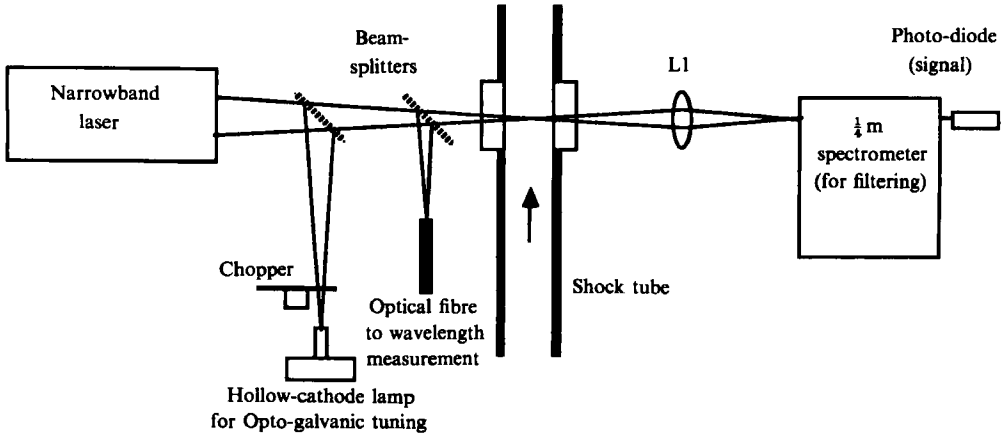

FIGURE 3. Experimental arrangement for narrowband absorption: L1: glass spherical lens, $f = 200$ mm; dye laser wavelength range: 560–600 nm.

wavelengths separated as far as possible. In this experiment the lower wavelength was obtained using a Spectra-Physics Model 165 argon-ion laser emitting at 488.0 nm while the higher wavelength was obtained using a Liconix Diolite diode laser emitting in the near infra-red at 770.0 nm.

3.4. *Absorption*

For the absorption experiment a Coherent cw Ring-dye laser pumped by a Spectra-Physics 2030 argon-ion laser was used to examine the desired absorption line. The dye laser was operated with Rhodamine 6G tunable over the wavelength range 560–600 nm and with bandwidth narrower than 20 MHz, much narrower than the absorption profiles probed here. The two transition lines of interest are at 585.249 nm and 594.483 nm, corresponding to transitions $1s_2 - 2p_1$ and $1s_5 - 2p_4$ (Paschen notation) with oscillator strengths given by Wiese, Smith & Miles (1969) as 0.123 and 0.0556 respectively.

For measurements in the precursor and relaxation zones, where it was necessary to tune the laser to line centre, the wavelength was determined optogalvanically and monitored during the shot to ensure there was no drift. For measurements in the quasi-equilibrium zone, approximately ten shots were used for each line, each with a slightly different detuning to measure the line profile. The wavelength was measured using a wavemeter which compares the wavelength of the dye laser to the known wavelength of a stabilized helium-neon laser. This measurement is accurate to ± 0.001 nm.

The experimental arrangement is shown in figure 3. The laser light was passed across the end of the shock tube and onto a fast-response photodiode. A quarter-metre spectrometer was used to ensure that only laser light contributed significantly to the absorption signal. Some problems were encountered maintaining consistent shock speeds for the measurements in the quasi-equilibrium zone. To ensure consistency between shots results were only used where the shock speed deviated from the mean by less than 5%.

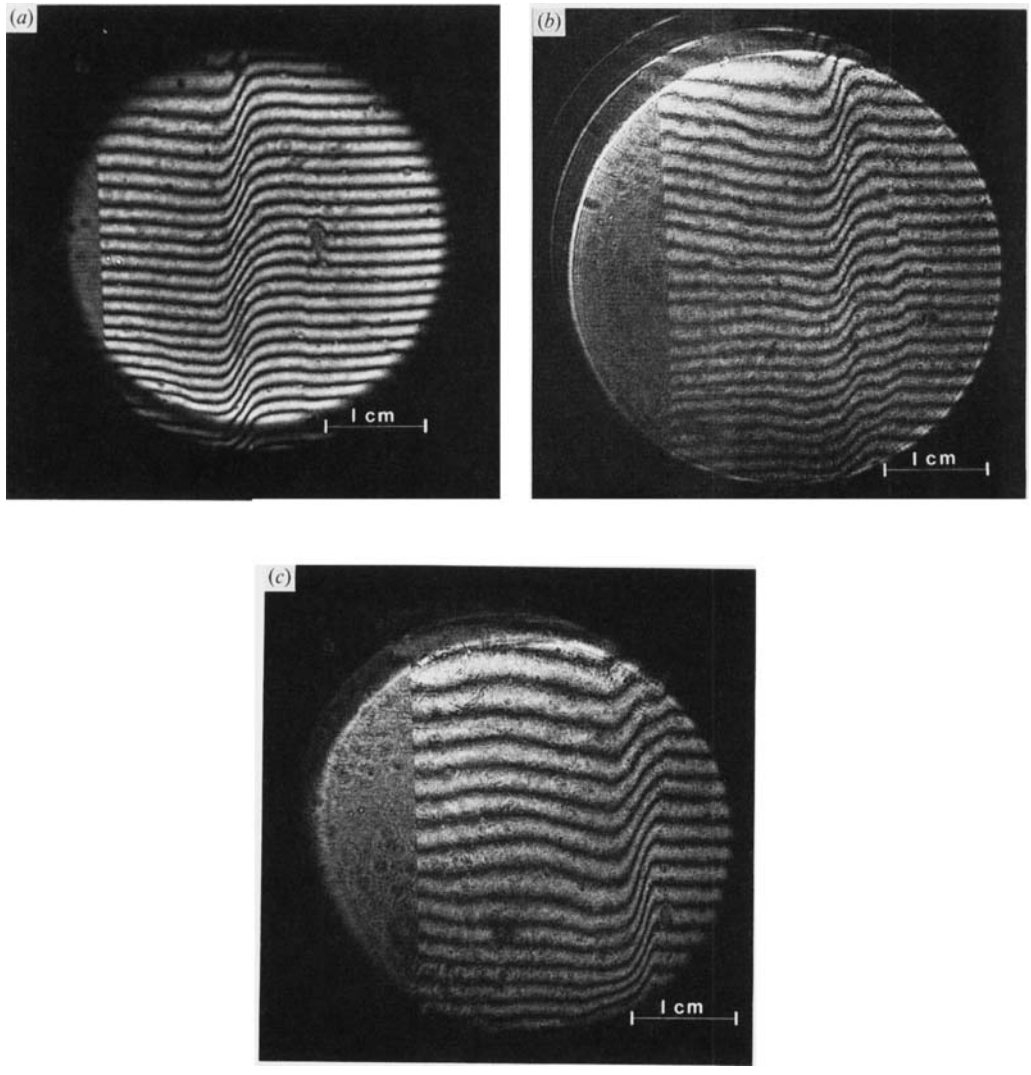

FIGURE 4. Spatially resolved interferograms displaying electron cascade fronts in neon. Flow is moving from left to right. Shock is to the right of the electron cascade front. (*a*) Flow classified as stable: $p_0 = 1.33$ kPa, $u_s = 8.49$ km/s. (*b*) Flow classified as unstable: $p_0 = 1.33$ kPa, $u_s = 8.87$ km/s. (*c*) Flow classified as unstable: $p_0 = 1.33$ kPa (0.2%H_2), $u_s = 8.92$ km/s.

4. Results and discussion

4.1. *Flow visualization*

Spatially resolved interferograms of the flow behind shock waves in neon are shown in figure 4. A summary of all flow visualization photographs recorded is given in table 2. Figure 4(*a*) is an interferogram of a stable flow within which a uniform one-dimensional electron cascade front is evident. Because of the low refractivity of neon atoms, the fringe shift across the shock front is difficult to observe. Like flows of argon and krypton, shock waves in neon are also observed to become unstable. Figure 4(*b*) shows a typical interferogram of unstable conditions where the ECF is no longer uniform. An extra negative-going fringe shift is observed propagating ahead of the ECF which, because of its size, could only be caused by an early liberation of

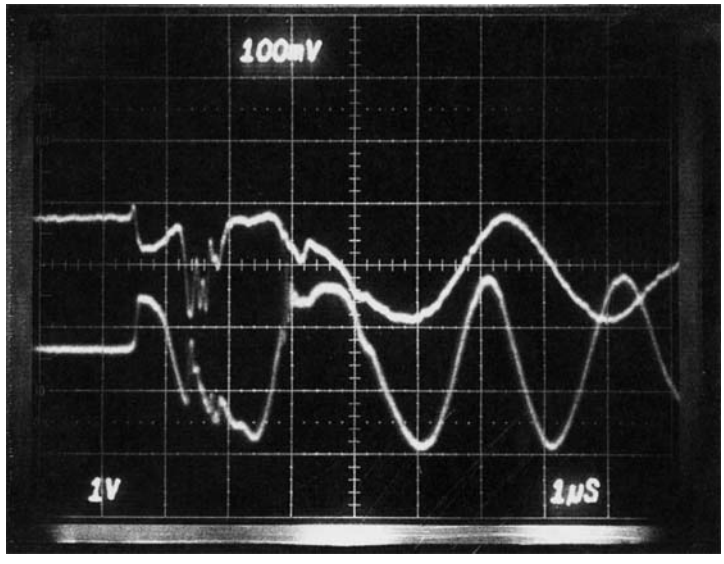

FIGURE 5. Fringe measurements. Upper trace is λ_1, lower trace is λ_2. $p_0 = 1.33$ kPa, $u_s = 9.07$ km/s, $\lambda_1 = 488.0$ nm, $\lambda_2 = 770.0$ nm.

Shock tube conditions				
Initial pressure (±0.01 kPa)	Gas type	Shock velocity (±0.05 km/s)	Shock Mach number	Classification: stable (S)/ unstable (U)
0.133	Ne	11.43	25.2	S
0.665	Ne	8.45	18.6	S
0.665	Ne	9.11	20.1	S
0.665	Ne	9.12	20.1	S
0.665	Ne	10.17	22.4	S
1.33	Ne	8.49	18.7	S
1.33	Ne	8.61	19.0	S
1.33	Ne	8.65	19.1	S
1.33	Ne	8.66	19.1	S
1.33	Ne	8.66	19.1	U
1.33	Ne	8.69	19.2	S
1.33	Ne	8.75	19.3	U
1.33	Ne	8.79	19.4	U
1.33	Ne	8.87	19.5	U
1.33	Ne	8.91	19.6	U
1.33	Ne	8.95	19.7	U
1.33	Ne	9.00	19.8	U
1.33	Ne/H_2 (1%)	8.78	19.4	U
1.33	Ne/H_2 (2%)	8.54	18.8	S
1.33	Ne/H_2 (2%)	8.88	19.6	U
1.33	Ne/H_2 (2%)	8.92	19.7	U

TABLE 2. Flow visualization results

Shock tube initial pressure (±0.01 kPa)	Shock velocity (±0.05 km/s)	Relaxation length		Peak electron pop.	
		Exp. (±0.1 cm)	Theory† (cm)	Exp. (±0.5 × 10^{17} cm^{-3})	Theory† (10^{17} cm^{-3})
0.665	8.48	2.1	3.7	1.7	1.8
0.665	8.57	1.9	3.4	1.9	1.9
1.33	8.02	2.0	2.8	2.3	2.5
1.33	9.07	1.3	1.2	3.8	4.5
1.33	9.26	1.2	1.0	4.5	4.9

† Using $S^*_{Ne-Ne} = 8.0 \times 10^{-20}$ cm^2/eV

TABLE 3. Relaxation lengths in neon

electrons. Results for all flow interferograms show a very definite shock velocity (for an initial pressure of 1.33 kPa) above which all shock waves were observed to be unstable. This value, at about 8.7 km s^{-1}, does not apply at lower initial pressures where all flows were classified as stable.

The addition of hydrogen to the argon test gas was observed by Glass & Liu (1978) to stabilize the flow. Figure 4(*c*) shows an interferogram where a similar amount of hydrogen (0.2% H_2 by volume) has been added to the test gas. The relaxation length appears to be reduced, as expected, but perturbations still exist, although significantly smaller than for the pure-test-gas cases. All flows where hydrogen was added were classified as unstable, except for one which fell within the stable regime for pure test gases anyway.

The source of such instabilities is yet to be determined. The sharp boundary between stable and unstable conditions seems to indicate a process such as interference by the driver gas or expansion fan created as the bursting of the diaphragm. Both of these possibilities were investigated but such disturbances were thought to be well behind the shock front and away from regions of instability. Investigations in argon, krypton, and neon all indicate that the observed instabilities are associated with a resolvable non-equilibrium zone. Destabilizing effects due to exothermic reaction sequences have been shown by Houwing *et al.* (1986) and McIntyre *et al.* (1989) to be unlikely to cause the instability. We can therefore only conclude that the non-equilibrium zone acts to amplify, or at least, not attenuate disturbances present in the flow. Bristow (1971) suggested this type of sequence whereby the non-equilibrium zone acted as a resonant cavity. Disturbances initiated by irregularities in the shock tube inner wall or by the boundary layer may be amplified, destabilizing the flow. Further experimental and theoretical work is required to investigate the validity of this type of hypothesis.

4.2. *Dual-wavelength interferometry*

A typical pair of experimental fringe shifts for the dual-wavelength interferometry are shown in figure 5. The upper trace is that of the blue laser at 488.0 nm while the lower trace is the red laser at 770.0 nm. Both exhibit a small jump where the shock passes followed by reversal in fringe direction where the electrons start to decrease the path length in the test arm. The passing of the electron cascade front is noted where there is a sudden shift of several fringes and this is followed by a slow increase in fringe shift as the gas cools in the quasi-equilibrium zone. In some cases, the fringes at the electron cascade front are unresolvable because of the high spatial frequency

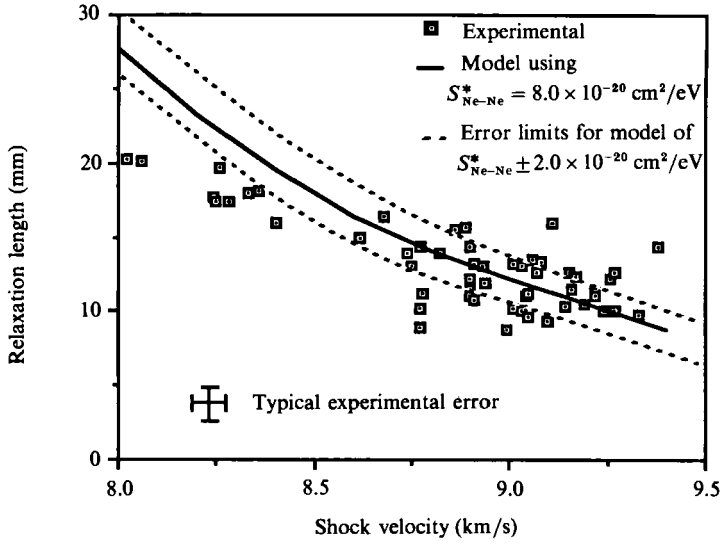

FIGURE 6. Relaxation length behind shock waves in neon, $p_0 = 1.33$ kPa.

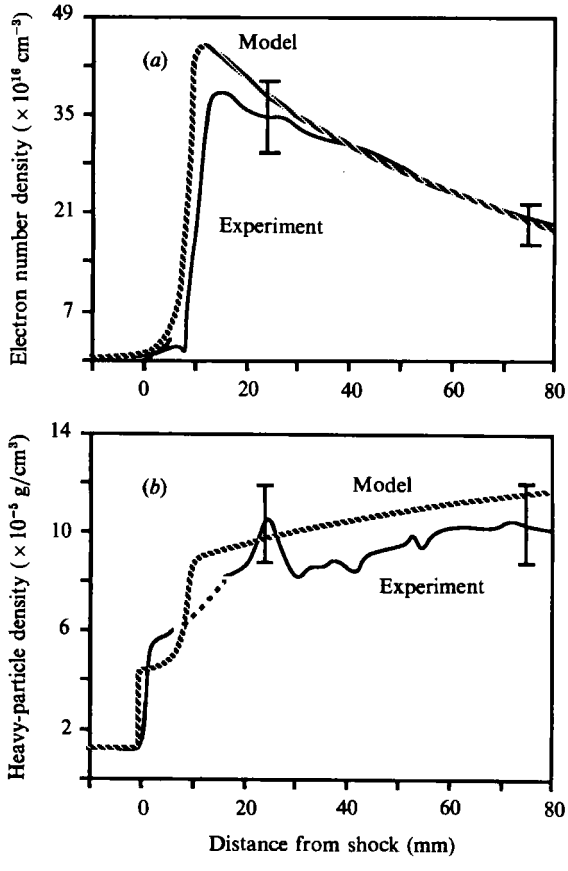

FIGURE 7. Variation of particle densities behind a shock wave in neon: $p_0 = 133$ kPa, $u_s = 9.07$ km/s. (*a*) Electron number density, (*b*) Heavy-particle density.

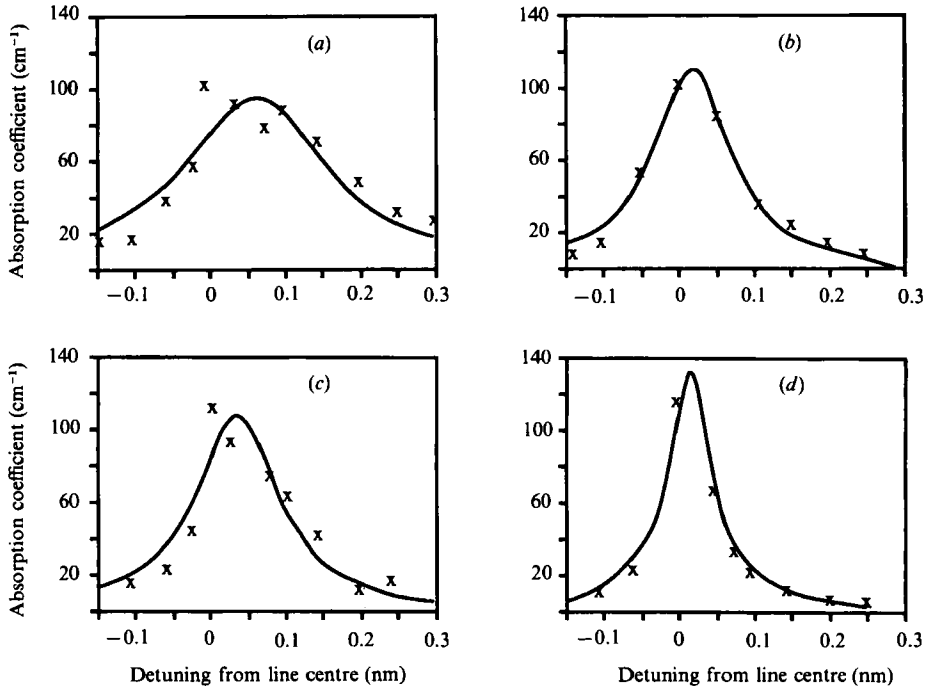

FIGURE 8. Typical fit of a Lorentzian profile to absorption measurements in neon. Distance behind shock: (*a*, *b*) 30 mm; (*c*, *d*) 60 mm. (*a*, *c*) $p_0 = 1.33$ kPa, $u_s = 9.1$ km/s, $1s_2$ level, $\lambda_0 = 585.249$ nm. (*b*, *d*) $p_0 = 1.33$ kPa, $u_s = 8.6$ km/s, $1s_5$ level, $\lambda_0 = 594.483$ nm.

$1s_5$ metastable level $\lambda = 594.483$ nm		$1s_2$ non-metastable level $\lambda = 585.249$ nm	
Shock speed (km/s)	Detuning (nm)	Shock speed (km/s)	Detuning (nm)
8.28	−0.150	8.82	−0.250
8.26	−0.100	8.90	−0.200
8.77	−0.050	9.06	−0.150
8.70	−0.025	9.10	−0.100
8.74	0.000	9.03	−0.050
9.04	+0.025	8.75	−0.025
8.90	+0.050	8.91	0.000
8.76	+0.075	9.01	+0.025
8.36	+0.100	9.03	+0.050
8.40	+0.150	8.94	+0.075
8.68	+0.200	9.22	+0.100
8.25	+0.250	9.16	+0.150
		9.27	+0.200
		9.38	+0.300
		9.22	+0.350
		9.17	+0.400
$u_{av} = 8.60$		$u_{av} = 9.07$	

TABLE 4. Summary of shock tube shots used for the experimental determination of the excited-state populations, linewidths, and line shifts in the quasi-equilibrium zone

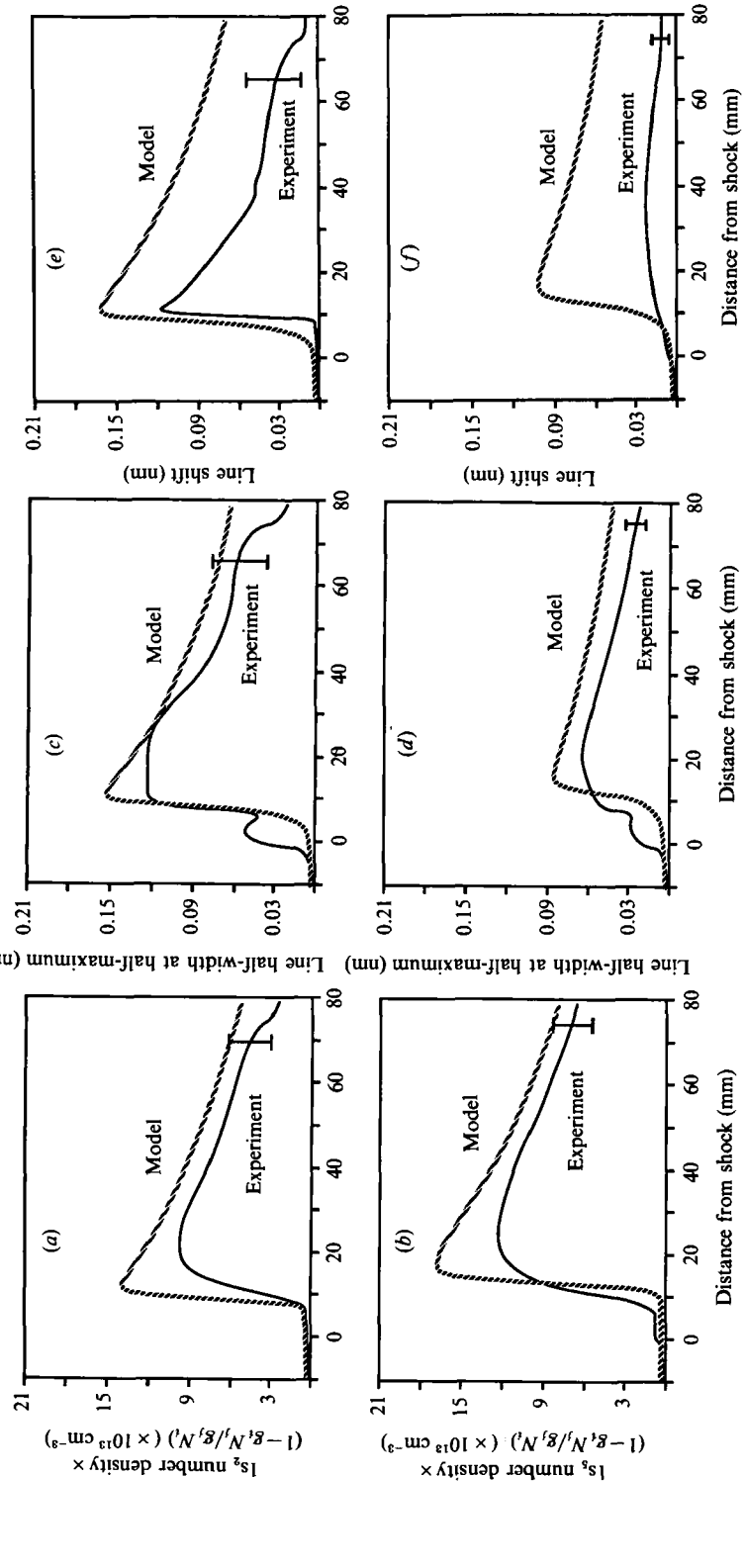

FIGURE 9. (*a*, *b*) Excited-state populations in the quasi-equilibrium zone behind shock waves in neon. (*a*) $p_0 = 1.33$ kPa, $u_s = 9.1$ km/s, $1s_2$ level, $\lambda_0 = 585.249$ nm. (*b*) $p_0 = 1.33$ kPa, $u_s = 8.6$ km/s, $1s_5$ level, $\lambda_0 = 594.483$ nm. (*c*, *d*) Absorption line half-widths at half-maximum in the quasi-equilibrium zone behind shock waves in neon. (*c*) $p_0 = 1.33$ kPa, $u_s = 9.1$ km/s, $1s_2$ level, $\lambda_0 = 585.249$ nm. (*d*) $p_0 = 1.33$ kPa, $u_s = 8.6$ km/s, $1s_5$ level, $\lambda_0 = 594.483$ nm. (*e*, *f*) Absorption line shifts in the quasi-equilibrium zone behind shock waves in neon. (*e*) $p_0 = 1.33$ kPa, $u_s = 9.1$ km/s, $1s_2$ level, $\lambda_0 = 585.249$ nm. (*f*) $p_0 = 1.33$ kPa, $u_s = 8.6$ km/s, $1s_5$ level, $\lambda_0 = 594.483$ nm.

of the fringe shift across the front and the limited spatial resolution of the detection system. Under these conditions, measurements are made where the fringes are visible and an integral number of fringes added for the region where the fringes disappear. The value of this integer is determined by comparing results with the theoretical model. No generality is lost as an incorrect choice of the integer introduces errors in the heavy particle and electron populations of the order of 100 %. This is far too large to be compensated for by other choices of parameters being used in the model.

Table 3 summarizes the results over a variety of fill pressures and shock speeds, showing the experimentally determined relaxation lengths (x_E) and peak electron populations ($N_{e,E}$). Using a value of $S^*_{Ne-Ne} = (8.0 \pm 2.0) \times 10^{-20}$ cm^2/eV we obtain the theoretical results for x_E and $N_{e,E}$ also shown in the table. This value was determined by collating all shots in neon where a relaxation length could be measured. Figure 6 shows a graph of all such points together with a curve of best fit predicted by the theoretical model, varying S^*_{Ne-Ne}. While the fit for the relaxation length is good for the faster speeds at higher fill pressures, relaxation lengths are shorter than expected at the other lower pressure or lower shock velocity conditions. It is not known at this stage whether this is due to the errors in the model, boundary-layer effects, or impurities in the shock tube. Liu (1979) has noted that boundary-layer effects can contribute to reducing the relaxation length in smaller cross-section tubes. Also we note that the effect of impurities may become more significant at the lower shock speeds and lower initial pressures where ionization due to atom–atom collisions will be slower. Impurities that have a much lower ionization potential will still contribute to the process, maintaining the relaxation length at a value smaller than expected.

A comparison of the measured excitation cross-section constant for neon with those of argon and krypton shows the value for neon to be slightly lower. Drawin & Emard (1973) have calculated rate coefficients for atom–atom excitation and ionization of noble gas atoms. The present results over a wide range of temperatures and, when expressed in the form of equation (2), give good comparisons with the experimentally measured values for argon and krypton. For neon they calculate $S^*_{Ne-Ne} = 7.0 \times 10^{-20}$ cm^2/eV, which is also in good agreement with the value measured here.

Figure 7 shows a comparison between the experimental data and the mode for the electron and heavy-particle populations throughout the flow. The agreement for both is quite good with the rate at which the gas cools justifying the radiation model used in the quasi-equilibrium zone. Errors in the heavy-particle plot are larger than those for the electron population as the heavy particles produce only a relatively small fringe shift. A heavy-particle population is not calculated in the region where the fringes disappear as matching between the two wavelengths is crucial and impossible to achieve without introducing large errors.

4.3. *Absorption*

The results for this section are divided into three subsections – the precursor, relaxation and equilibrium zones. The results for the equilibrium zone are presented first as the results from this region contribute to the theory for the other regions.

4.3.1. *Equilibrium zone*

A summary of the shock tube shots used to determine the two absorption line profiles is shown in table 4. The results for each shot were digitized and a Lorentzian curve was fitted to points every 2 mm behind the shock. A best fit was obtained by

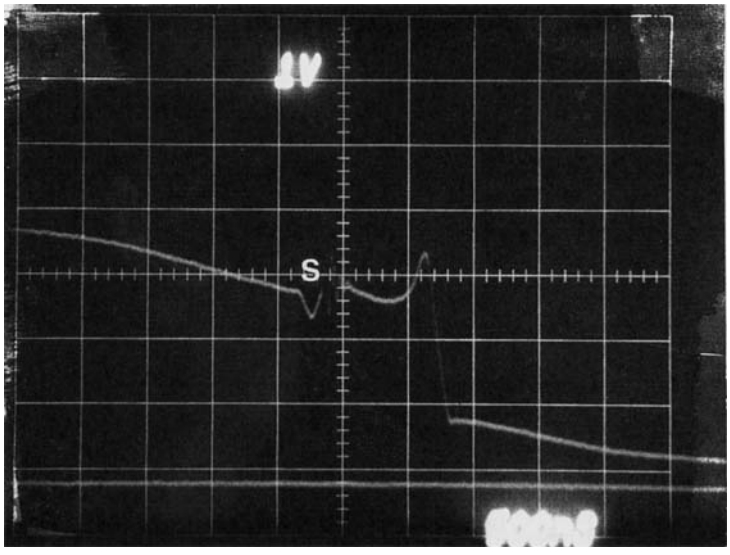

FIGURE 10. Absorption of tuned radiation by excited neon atoms. $p_0 = 1.33$ kPa; upper trace in each is intensity $I(t)$; lower trace $I(t) = 0$. S indicates time of arrival of the shock wave. Timescale is: 500 ns/division. $\lambda_0 = 585.249$ nm, $u_s = 9.14$ km/s.

varying the line half-width-at-half-maximum, the line shift, and the absorbing energy level's population. A typical fit at two points behind the shock front is shown in figure 8. The profile is small in the relaxation zone where few electrons exist and other broadening mechanisms dominate. The profile grows dramatically at the ECF where the high electron population introduces large Stark widths and shifts. From then on, the profile slowly decreases as the gas cools.

Results of the curve fitting for the three parameters compared with theoretical calculations (equations (6), (17*a*, *b*)) are shown in figure 9. In calculating the flow parameters for these equations, the model using the new $S^*_{\mathrm{Ne-Ne}}$ has been used. As can be seen, the fit in most cases is good, reinforcing theoretical calculations in the equilibrium zone of the excited-state population by Oettinger & Bershader (1967) and Stark parameter by Griem (1974). The population measurements show a slight deviation from that expected near the ECF. There are two possible explanations for this. Firstly, shot to shot variations in the shock speed causes the peak of the ECF to be at different distances behind the shock front from different shots. Consequently the Lorentzian fit to the data is not good in this region. Secondly there is a large excited-state population in this region and this causes the plasma to become optically thick near line centre. Larger errors are then introduced in calculating the absorption coefficient, resulting in errors in the fit and the excited-state population.

Linewidths calculated for both lines are in excellent agreement with the theory. However, the shifts observed were much smaller than expected. Wiese (1965) notes that variations in linewidths and shifts have been observed for argon. In particular some of the calculated shifts have been unreliable and we presume this may also be the case for neon.

4.3.2. *Precursor zone*

A typical absorption trace for this region is shown in figure 10. Before the shock arrives there is a gradual increase in the absorption as the excited states are populated by reactions initiated by precursor radiation. When the shock front

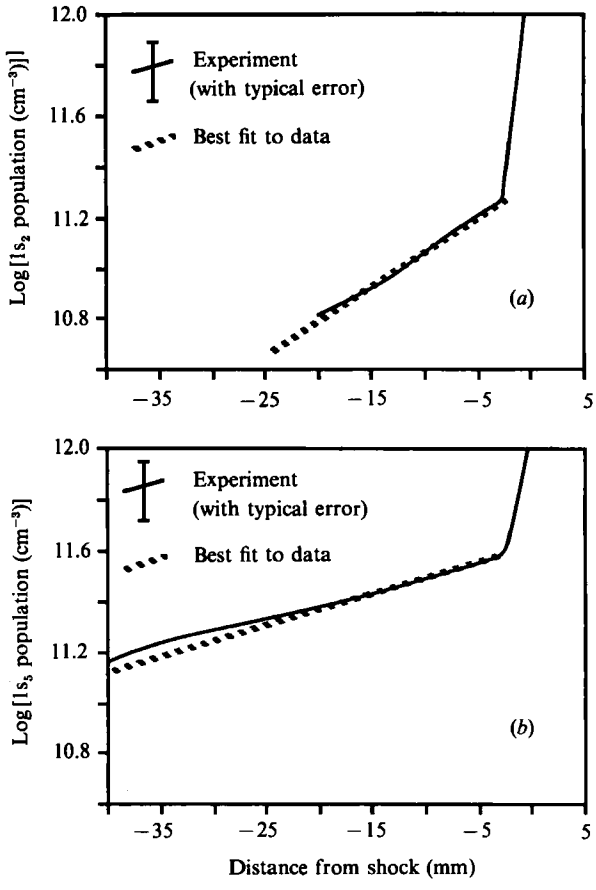

FIGURE 11. Excited-state populations in the precursor zone ahead of shock waves in neon. (*a*) $p_0 = 1.33$ kPa, $u_s = 9.14$ km/s, $1s_2$ level, $\lambda_0 = 585.249$ nm. (*b*) $p_0 = 1.33$ kPa, $u_s = 8.74$ km/s, $1s_5$ level, $\lambda_0 = 594.483$ nm.

passes, there is a jump as the gas is compressed and then there is a rapid increase in the absorption as the population builds up throughout the relaxation zone. The absorption behind the ECF is almost total as there is a comparatively large excited-stated population. Figure 11 shows the populations calculated from these traces. The narrow linewidths in this region of the flow do not allow an experimental determination of the line shape. Hence linewidths are calculated using the theory presented in §2.3.

The results exhibit a roughly exponential decrease in the population away from the shock front. This suggests a fit to the data of the form

$$N_{ex}(x) = N_{ex}(0) \exp\left[\frac{-t}{T_0}\right], \tag{21}$$

where $N_{ex}(0)$ is the excited-state number density at the shock front, t is the time until the shock front passes the observation point and T_0 is a constant. This form is the same as that fitted to precursor populations in krypton by Bötticher & Kilpin (1984). Table 5 lists the values for the parameters of (21) determined in this experiment. Models have been developed to predict the populations ahead of the shock but these

Shock speed (km/s)	λ (nm)	Energy level	$N_{ex}(0)$ (10^{17} cm^{-3})	T_0 (μs)
8.74	594.483	$1s_5$	2.241	4.82
8.91	594.483	$1s_5$	2.457	5.03
8.99	585.249	$1s_2$	0.903	1.89
9.14	585.249	$1s_2$	1.246	1.72

TABLE 5. Absorption results in the precursor region. $N_{ex}(0)$ is the excited-state population immediately before the shock front, and T_0 is a constant determining the rate at which the population decreases away from the shock.

usually do not consider metastable levels. Bötticher & Kilpin proposed that the sum of the population of the metastable $1s_5$ level and the non-metastable $1s_4$ level can be compared with the theoretical excited-state population $N_{ex}(0)$. Considering conditions with the same initial fill pressure and shock Mach number they conclude that their results are within a factor of five of the model calculations. If we proceed in a similar manner here, but instead add the $1s_2$ and $1s_5$ populations together, we obtain $N_{ex}(0) = 3.4 \times 10^{17}$ m^{-3} for conditions of an initial pressure of 1.37 kPa and $M \approx 20$. This is considerably lower than the values presented in Bötticher & Kilpin of $N_{ex}(0) = 3.3 \times 10^{18}$ m^{-3} for argon and $N_{ex}(0) = 5.5 \times 10^{18}$ m^{-3} for krypton. However, the energy of these excited states for neon is 16.7 eV as compared to 11.6 eV for argon and 10.0 eV for krypton, implying that stronger shocks are required to obtain similar precursor populations. Also of note is that the values obtained for T_0 for neon are $\frac{1}{4}$ to $\frac{1}{2}$ of that for krypton. These data seem to indicate that the penetration of the precursor radiation is far less for neon as the population drops at a faster rate the further one looks ahead of the shock. However, we should note that our experiments looked only about 3 cm ahead of the shock while those for krypton looked of the order of 15 cm ahead.

4.3. *Relaxation zone*

As with measurements in the precursor zone, linewidths for this region have been taken from theoretical consideration. McIntyre *et al.* (1989) have found that these predictions are reasonably accurate for argon and hence are presumed not to introduce too large an error here. Figure 12 showed excited-state populations calculated from absorption traces like that in figure 10 compared with theoretically predicted populations from equation (6). The theoretical curves show the excited-state populations as being very low in the relaxation zone, but rising steeply to maximum values near the electron cascade front. Throughout the non-equilibrium zone, the experimentally measured population is several orders of magnitude higher than expected. McIntyre *et al.* noted a similar effect in argon and proposed that in fact, electrons have insufficient energy to ionize the excited states of the atom. A revised model was proposed whereby, in the early part of the relaxation zone, further collisions with atoms were responsible for ionization. Similar calculations may be carried out for neon, further details of which can be found in McIntyre (1989).

It should be noted that, while higher excited-state populations behind shock waves in neon were observed at unstable conditions, similar observations in argon were made at stable conditions. The populations measured fall well below those required for anomalous relaxation as proposed by Yushchenkova (1980) and seem unlikely to be responsible for the instability process.

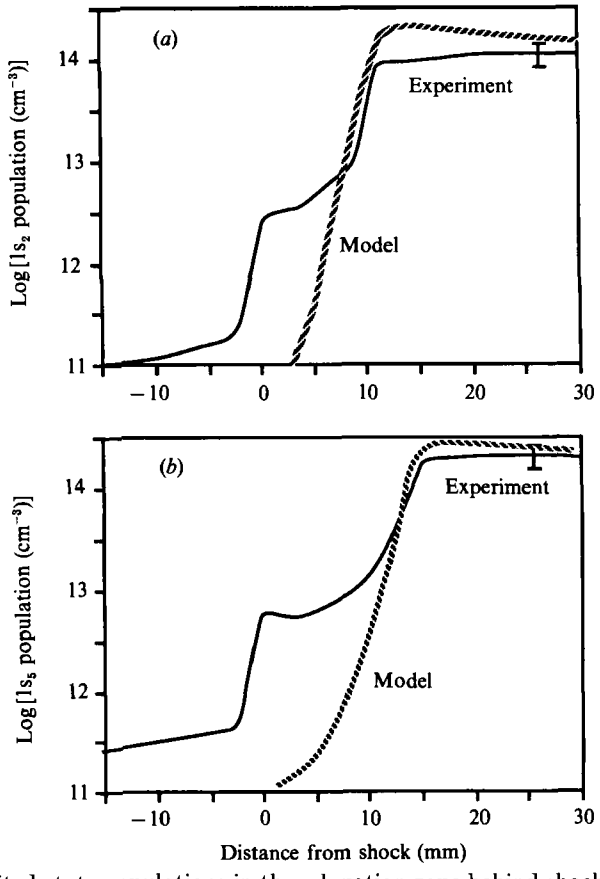

FIGURE 12. Excited-state populations in the relaxation zone behind shock waves in neon. (*a*) $p_0 = 1.33$ kPa, $u_s = 9.14$ km/s, $1s_2$ level, $\lambda_0 = 585.249$ nm. (*b*) $p_0 = 1.33$ kPa, $u_s = 8.74$ km/s, $1s_5$ level, $\lambda_0 = 594.483$ nm.

5. Conclusions

The relaxation processes behind shock waves in ionizing neon have been observed by monitoring concentrations of atoms, electrons, and excited atoms. The atom–atom excitation cross-section constant for neon at these conditions has been found to be $(8.0 \pm 2.0) \times 10^{-20}$ cm^2/eV. Measured atom and electron densities have been found to be in good agreement with the currently accepted ionization model using this value.

Absorption measurements have shown experimentally measured populations of excited states to be in good agreement with theory in the quasi-equilibrium zone. Linewidths measured in this zone were also found to be in good agreement with theory. However, excited-state populations were found to be several orders of magnitude higher than expected in the non-equilibrium zone. It is proposed that this results from ionization initially occurring by the slower process of collisions with atoms rather than by collisions with electrons. There are insufficient energetic electrons to sustain this process until later within the relaxation process.

Shock waves in neon are found to become unstable for shocks with velocities greater than 8.7 km/s propagating into ambient pressures of 1.33 kPa. The cause of this instability is yet to be explained but seems to be associated with the non-equilibrium process.

Further work required includes extending the relaxation model for neon to incorporate the effects of impurities and the boundary layer. Both of these processes can reduce the relaxation zone, resulting in an overestimate of the atom–atom excitation cross-section constant. Further work could also be conducted into identifying possible sources of disturbances which may disrupt the flow.

The authors gratefully acknowledge Mr Ian Darroch and Mr Paul Walsh for their competent operation of the shock tube and ancillary equipment. We are also grateful to Dr Don Bone and Dr Paul Taloni for their practical assistance and their positive contributions through discussions of the experimental results. This work was financially supported by the Australian Research Council.

REFERENCES

ALIEVA, I. A. & ANDREEV, E. A. 1987 *Zh. Tekh. Fiz.* **57**, 1172–1174.

ALPHER, R. A. & WHITE, D. R. 1959 *Phys. Fluids* **2**, 162–169.

BARYSHNIKOV, A. S. & SKVORTSOV, G E. 1979 *Zh. Tekh, Fiz.* **49**, 2383–2485. (Transl. *Sov. Phys. Tech. Phys.* **49**, 1401–1402.)

BATES, D. R., KINGSTON, A. E. & MCWHIRTER, R. W. P. 1962 *Proc. R. Soc. Lond.* A**267**, 297–312.

BEDIN, A. P. 1989 *Zh. Tekh. Fiz.* **59**, 152–155.

BÖTTICHER, W. & KILPIN, D. 1984 *Exp. Fluids* **2**, 177–181.

BÖTTICHER, W., MÜLLER, B.-H. & SCHNEIDER, J.-M. 1981 In *15th Intl Conf. Phenomena of Ionized Gases, Minsk*, P-0801.

BRISTOW, M. P. F. 1971 *UTIAS Rep.* 158.

BYRON, S., STABLER, R. C. & BORTZ, P. I. 1962 *Phys. Rev. Lett.* **8**, 376–379.

DEMMIG, F. 1977 In *Proc. 11th Intl Symp. Shock Tubes and Waves, Seattle.*

DEMMIG, F. 1983 In *Proc. 14th Intl. Symp. Shock Tubes and Waves, Sydney.*

DRAWIN, H. W. & EMARD, F. 1973 *Phys. Lett.* **43**, A333.

FOWLES, G. R. & HOUWING, A. F. P. 1984 *Phys. Fluids* **27**, 1982–1990.

GLASS, I. I. & LIU, W. S. 1978 *J. Fluid Mech.* **84**, 55–77.

GLASS, I. I., LIU, W. S. & TANG, F. C. 1977 *Can. J. Phys.* **55**, 1269–1279.

GRIEM, H. R. 1964 *Plasma Spectroscopy*. McGraw-Hill.

GRIEM, H. R. 1974 *Spectral Line Broadening by Plasmas*. Academic.

GRIGOR'EV, V. G., MISHIN, G. I., YUSCHENKOVA, N. I. & ROSCHIN, O. V. 1986 *Pis'ma Zh. T.* **12**, 224–231.

HANSEN, R. K., SALIMIAN, S. & REA, E. C. 1983 *Proc. 14th Symp. Shock Tubes and Waves, Sydney*, pp. 594–601.

HARWELL, K. E. & JAHN, R. G. 1964 *Phys. Fluids* **7**, 214–222.

HENDERSON, L. F. 1987 *Proc. 16th Intl Symp. Shock Tubes and Waves, Aachen*, pp. 261–266.

HENDERSON, L. F. 1988 *J. Fluid Mech.* **189**, 509–529.

HOFFERT, M. I. & LIEN, H. 1967 *Phys. Fluids* **10**, 1769.

HORN, K. P., WONG, H. & BERSHADER, D. 1967 *J. Plasma Phys.* **1**, 157–170.

HOUWING, A. F. P., FOWLES, G. R. & SANDEMAN, R. J. 1983 In *Proc. 14th Intl Symp. on Shock Tubes & Waves, Sydney*, pp. 277–284.

HOUWING, A. F. P., MCINTYRE, T. J., TALONI, P. A. & SANDEMAN, R. J. 1986 *J. Fluid Mech.* **170**, 319–337.

ITIKAWA, Y. 1974 *Atomic Data and Nuclear Data Tables*, Vol. 14, p. 1.

KELLY, A. J. 1966 *J. Chem. Phys.* **45**, 1723.

KUZNETSOV, N. M. 1986 *Zh. Eksp. Teo.* **91**, 1325–1330.

KUZNETSOV, N. M. 1990 *Usp. Fiz. Nav.* **159**, 493–527.

KUZNETSOV, N. M. & SARROV, S. D. 1989 *Dokl. Akad. Nauk. SSSR* **306**, 1106–1110.

LEONARD, D. J. 1974 *Atomic Data and Nuclear Data Tables* vol. 14, p. 22.

LIU, T. P. 1986 *Commun. Pure Appl. Maths* **39**, 565–594.

LIU, W. S. 1979 *UTIAS Rep.* 226.

LIU, W. S. & GLASS, I. I. 1979 *J. Fluid Mech.* **91**, 679–696.

LIU, W. S., TAKAYAMA, K. & GLASS, I. I. 1980 *J. Fluid Mech.* **97**, 513–530.

LIU, W. S., WHITTEN, B. T. & GLASS, I. I. 1978 *J. Fluid Mech.* **87**, 609–640.

MCINTYRE, T. J. 1989 Ph.D. Thesis, Australian National University.

MCINTYRE, T. J., HOUWING, A. F. P., BACHOR, H.-A. & SANDEMAN, R. J. 1987 In *Proc. 16th Intl Symp. Shock Tubes and Waves, Aachen*; pp. 161–168.

MCINTYRE, T. J., HOUWING, A. F. P., BACHOR, H.-A. & SANDEMAN, R. J. 1989 In *Proc. 17th Intl Symp. Shock Tubes and Waves, Bethlehem, PA.*

MCLAREN, T. I. & HOBSON, R. M. 1968 *Phys. Fluids* **11**, 2162–2172.

MACHADO, L. E., LEAL, E. P. & CSANAK, G. 1984 *Phys. Rev.* A **29**, 1811–1824.

MEYER-PRÜSSNER, R. 1983 Ph.D. thesis, Universität Hannover.

MISHIN, G. I., BEDIN, A. P., YUSHCHENKOVA, N. I., SKVORTSOV, G. E. & RYAZIN, A. P. 1981 *Zh. Tekh. Fiz.* **51**, 2315–2324. (Transl. *Sov. Phys. Tech. Phys.* **26**, 1363.)

MUNZ, C.-D. 1987 In *Proc. 16th Intl Symp. Shock Tubes and Waves, Aachen*, pp. 685–691.

NI, A. L., SUGAK, S. G. & FORTOV, V. E. 1987 *High Temp. Res.* **24**, 435–440.

OETTINGER, P. E. & BERSHADER, D. 1967 *AIAA J.* **5**, 1625–1632.

PETSCHEK, H. & BYRON, S. 1957 *Ann. Phys.* **1**, 270–315.

PULFORD, D. P. 1987 Honours Thesis, Australian National University.

SANDEMAN, R. J. & ALLEN, G. H. 1971 *Proc. 8th Intl Shock Tube Symp.* Chapman & Hall.

TANG, F. C. 1977 *UTIAS Tech. Note* 212.

TRAVING, G. 1968 In *Plasma Diagnostics* (ed. W. Lochte-Holtgreven), pp. 66–134. North-Holland.

WIESE, W. L. 1965 In *Plasma Diagnostic Techniques* (ed. R. H. Huddlestone & S. L. Leonard), pp. 265–317. Academic.

WIESE, W. L., SMITH, M. W. & MILES, B. M. 1969 *Atomic Transition Probabilities*, vol. 22, p. 193. *Natl. Bur. Stand.*

WONG, H. & BERSHADER, D. 1966 *J. Fluid Mech.* **26**, 459–479.

YUSHCHENKOVA, N. I. 1980 *Pis'ma Zh. Tekh. Fiz.* **6**, 1283–1288. (Transl. *Sov. Tech. Phys. Lett.* **6**, 550.)

YUSHCHENKOVA, N. I., MISHIN, G. I. & ROSHCHIN, O. V. 1985 *Pis'ma Zh. Tekh. Fiz.* **11**, 517–524. (Transl. *Sov. Tech. Phys. Lett.* **11**, 215.)

ZAPESOCHNYI, I. P. & FELSTON, P. V. 1966 *Opt. Spectrosc.* **20**, 291.